Available online at www.sciencedirect.com
SCIENCE DIRECT®
Composites Science and Technology 65 (2005) 149–160
COMPOSITES SCIENCE AND TECHNOLOGY
www.elsevier.com/locate/compscitech

Characterization of fiber/matrix interface strength: applicability of different tests, approaches and parameters

Serge Zhandarov, Edith Mäder *

Institute of Polymer Research Dresden, Hohe Strasse 6, D-01069 Dresden, Germany

Received 26 November 2003; received in revised form 30 June 2004; accepted 5 July 2004
Available online 25 August 2004

Abstract

Different approaches to interface strength characterization in fibrous composite materials by means of micromechanical tests are analyzed. Special attention is paid to single fiber pull-out and microbond techniques. For these tests, advantages and disadvantages of stress-based and energy-based models of interfacial debonding and corresponding adhesional parameters (local interfacial shear strength, critical energy release rate, adhesional pressure) are discussed. The following analytical models developed to measure these parameters as well as to determine the interfacial frictional stress are considered in detail: (1) the use of the debond or "kink" force from the force–displacement curves; (2) two-parameter fit of experimentally measured maximum pull-out force as a function of embedded length; and (3) models assuming two-stage debonding with imperfect interface at the second stage. The analysis is illustrated by our own experimental data on adhesion of polymer and cement matrices to different reinforcement fibers.

Keywords: B. Debonding; B. Fiber–matrix bond; B. Interface; C. Failure criterion; Micromechanical tests

1. Introduction

Interface is the key region which determines, to a great extent, the set of properties of all heterogeneous systems, including composite materials. A typical composite consists of a continuous phase (the matrix) and inclusions of other phase(s) distributed within it (in the form of particles, fibers or elements having other shape). In this paper we shall consider composites in which the discontinuous phase is formed by fibers. As a rule, the strength of fibers in fibrous composites exceeds considerably the strength of the matrix, and therefore such composites are often spoken about as "fiber-reinforced composites" (FRC). The fibers ensure the strength of the material, while the matrix helps to keep the shape of the part; the interface, as a key element of the composite, transfers the load from the matrix to the fibers and, thus, it is responsible for the effect of "reinforcement".

Fiber-reinforced composites can be considered at four structural levels (Fig. 1). At the molecular level (Fig. 1(a)), the interaction between the two dissimilar phases, the fiber and the matrix, is determined by chemical structures of both phases and is due to van der Waals forces, acid–base interactions and chemical bonds (first of all, covalent ones). From chemical point of view, the strength of interfacial interaction depends on the surface concentration of interfacial bonds and the bond energies. Quantitatively, it is characterized by the work of adhesion, which includes the contributions of all types of physical and chemical interactions, both local (acid–base, covalent) and non-local, such as the van der Waals forces. At the micro level (single fibers, Fig. 1(b)), interfacial interaction is usually described in terms of various parameters which characterize load transfer through the interface: bond strength, interfacial

* Corresponding author. Tel.: +49 351 4658 305; fax: +49 351 4658 362.
E-mail address: emaeder@ipfdd.de (E. Mäder).

0266-3538/$ - see front matter © 2004 Elsevier Ltd. All rights reserved.
doi:10.1016/j.compscitech.2004.07.003

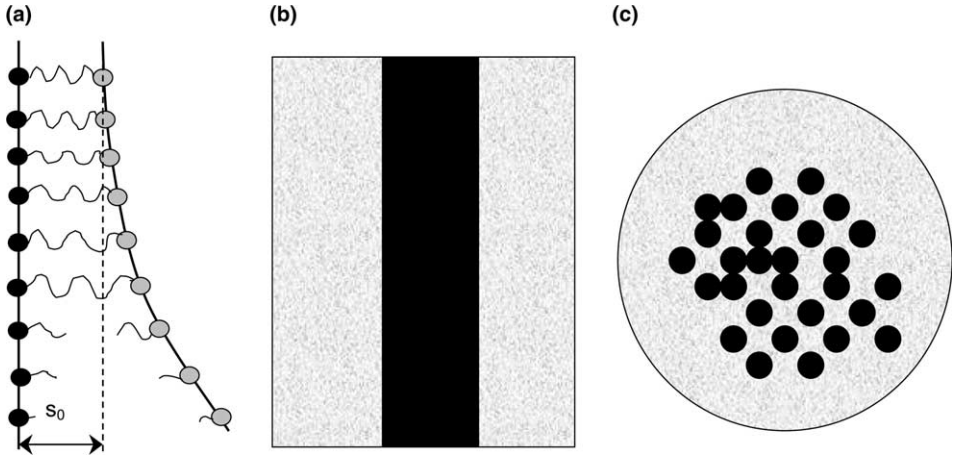

Fig. 1. Structural levels of a fiber-reinforced composite: molecular level (a), micro level (b) and meso level (c). The equilibrium interatomic distance is designated as s_0.

shear stress, critical energy release rate, etc. The meso level (Fig. 1(c)) takes into account the actual distribution of reinforcing fibers in the matrix and determines the structural element of the composite; and, finally, the macro level (not shown in Fig. 1) characterizes parts or, at least, the composite as bulk material.

The concept of interface is considered in the literature as regarding to the first two levels. At the molecular level, it is studied by chemistry and molecular physics, and the main subject of study is "fundamental adhesion" [1,2], including such aspects as the nature and surface density of adhesional bonds, their distribution in energy, ranges of action, etc. General questions related to surface energy are considered by thermodynamics. However, from the viewpoint of engineering, whose problems are stress transfer efficiency and interfacial strength [3,4], the micro level is the most important. Molecular aspects of interfacial science are often discussed in the literature as concerning the interface formation [5], while micromechanical ones are mentioned almost exclusively in concern with interfacial failure [6]. Bearing in mind that, in fact, molecular interactions at the interface directly affect interfacial strength [7,8] and, thus, separate consideration of the two levels is an oversimplification, we shall limit ourselves, in this paper, to the micromechanical description of the interface, particularly, the techniques used for the characterization of fiber/matrix interfacial properties. This approach includes three closely interrelated problems: (1) choice of interfacial parameters to be measured; (2) proper selection of micromechanical tests for the interface characterization; and (3) development of models to adequately relate test results to interfacial parameters, or, in other words, adequate data treatment. The aim of this paper is to review existing practice of interface strength characterization at the single fiber level and to select suitable procedures to determine fiber–matrix interfacial properties.

2. Micromechanical tests and interfacial parameters

2.1. General remarks

In order to determine parameters of interfacial interaction between fibers and matrices, quite a large number of various micromechanical tests have been developed. Under "micromechanical tests", we shall understand testing specimens containing single fiber. All such tests can be divided into two groups. One group includes tests in which external load is applied directly to the fiber (Fig. 2); these are, first of all, the single fiber pull-out test [9] (a) with its variations, such as microbond test [10] (b) and three-fiber test [11] (c), as well as the push-out test

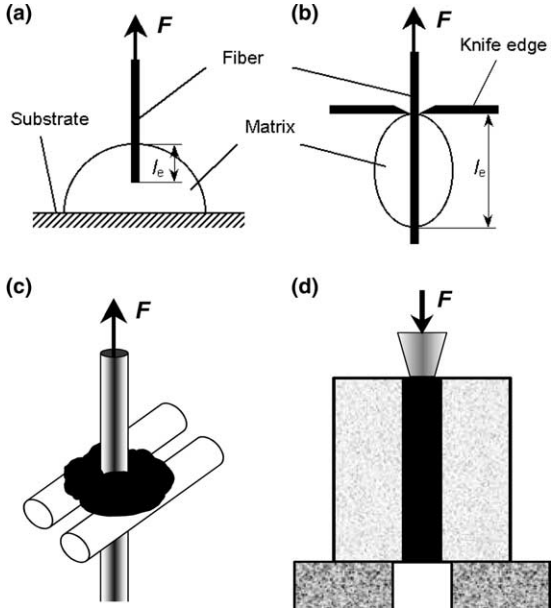

Fig. 2. Micromechanical tests in which external load is applied directly to the fiber: pull-out (a), microbond (b), three-fiber test (c), and push-out (d).

[12,13] (d). Another group is formed by tests with only matrix externally loaded (Fig. 3) – fragmentation test [14] (a), Broutman test [15] (b) and variations of the fragmentation test in which the matrix is subjected to bending rather than tension.

There are extensive discussions in the literature about how adequate is each different micromechanical test for interface characterization. It is obvious that, in an adequate test configuration, stress distribution must be similar to that in a real composite. For composites with ductile matrices and brittle fibers (i.e., the matrix elongation-to-break is several times greater than the fiber elongation-to-break, such as for carbon fiber reinforced polymers), it is the fragmentation test. On the contrary, for the composites based on brittle matrices, which fail through multiple transverse cracking (with reinforcing fibers bridging the cracks), the pull-out test appears to be closer to reality. However, as a tool for investigation of interfacial adhesion, it can be successfully used for the matrices with large elongation-to-break, too – under the condition that interfacial debonding occurs at not very large relative matrix deformation near the fiber.

There is an ample literature on theoretical and practical aspects of the fragmentation test [14,16–19]. In this paper, we shall consider predominantly the tests based on single fiber pull-out, which we consider to be especially interesting and important, because these allow to relate the load transfer ability of the interface to adhesional parameters at the molecular level [8,20–22]. The cases of "brittle" (cement) and "ductile" (polymeric) matrix will not be specially separated; however, the results obtained and the applicability of different models of the data treatment will be discussed taking into account particular mechanical properties of the components.

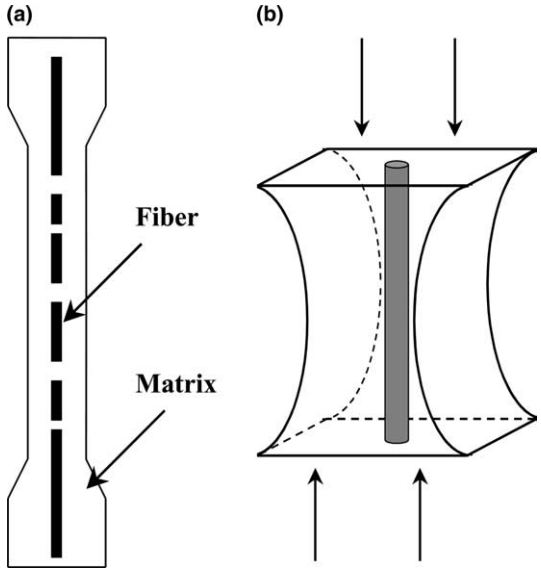

Fig. 3. Micromechanical tests in which external load is applied to the matrix: fragmentation test (a) and Broutman test (b).

2.2. Force–displacement curves and their interpretation

In the standard pull-out and microbond tests, the load applied to the fiber end is recorded as a function of the displacement of this end with respect to a "stationary" point in the specimen, usually at the substrate or grips holding the matrix. These two tests differ only by boundary conditions [23,24], and this difference can often be neglected [25], so that force–displacement curves from these two tests are very similar. In further analysis, we shall not distinguish the microbond and pull-out tests unless this is absolutely necessary. A typical force–displacement curve is shown in Fig. 4. It consists of three parts corresponding to the three stages of a pull-out test. At the first stage ($0 \leqslant F \leqslant F_d$), the fiber–matrix interface remains intact, and this part of the curve is nearly linear for a fiber–matrix system whose components considered to be linearly elastic. When the external load reaches some critical value ("debond force", F_d), the fiber begins to debond off the matrix through interfacial crack propagation [13,26]. At this second stage ($F_d \leqslant F \leqslant F_{max}$), the registered force continues increasing with the fiber end displacement (or with crack length), because frictional load in debonded regions is added to the adhesional load from the intact part of the interface. After a peak load, F_{max}, is reached, the crack propagation becomes unstable, the whole embedded length fully debonds and the measured force drops from F_{max} to F_b (see Fig. 4). From this moment and until complete pull-out, the "tail" force is due to frictional interaction between the fiber and the matrix.

The traditional way to characterize the quality of interfacial bonding is calculating the apparent interfacial shear strength (apparent IFSS, τ_{app}), according to the definition [10]

$$\tau_{app} = F_{max}/(\pi d_f l_e), \quad (1)$$

where d_f is the fiber diameter and l_e is the embedded length.

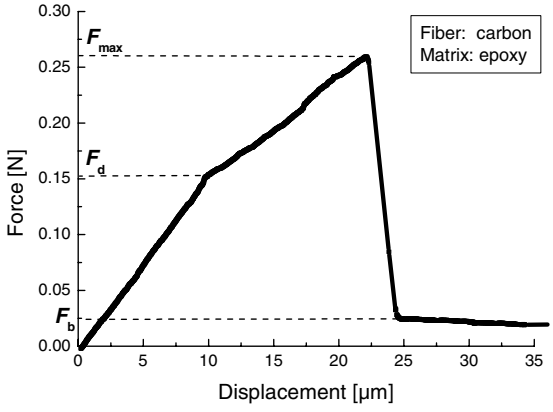

Fig. 4. A typical force–displacement curve recorded during a pull-out test.

The τ_{app} values calculated from Eq. (1) usually suffice to distinguish between "good" and "poor" bond strength and to estimate the efficiency of matrix and/or fiber surface modification (better/worse interfacial bonding). However, a quantitative characterization of the fiber–matrix interface properties requires a more adequate approach which should take into account the actual mechanism of interfacial failure and definitely include the following two requirements [27,28]:

- the use of *local* interfacial parameters instead of averaged or apparent ones;
- separation of the contributions of adhesion (sometimes referred in the literature as "chemical bonding") and friction.

For this purpose, numerous models describing stress distribution and interfacial failure in fiber–matrix systems have been proposed.

2.3. Theoretical models of interfacial failure in micromechanical tests

All these models can be classified into two major categories, depending on the basic assumption of the condition for debonding (with additional variations accounting for peculiarities of the debonding process in particular fiber–matrix systems).

2.3.1. Stress-controlled debonding

Stress-controlled debonding models are historically the first ones; these have been developed by many researchers [4,6,11,29,30]. In these models, the ultimate interfacial shear strength, τ_d (local shear stress near the crack tip, which is required to produce debonding) is supposed to be constant during the test (i.e., independent of the crack length, a). This is illustrated in Fig. 5, which shows interfacial shear stress distribution along the embedded fiber. Curve 1 corresponds to the moment of crack initiation; the interfacial shear stress is τ_d at the crack tip ($x = 0$) and decreases along the embedded length. Curve 2 presents shear stress distribution for an advanced stage of debonding (crack length $a = 50$ μm). In the debonded region ($x < a$), the shear stress is determined by interfacial friction and is assumed to be constant. In the intact zone, shear stress decreases from the same τ_d value; in other words, the peak value is constant and does not depend on the crack length. In this paper, we shall use our own model whose most detailed description can be find in [24,31,32]. It relates τ_d to the debond force, F_d, as

$$\tau_d = \frac{F_d \beta}{\pi d_f} \coth(\beta l_e) + \tau_T \tanh \frac{\beta l_e}{2}, \tag{2}$$

where β is the shear-lag parameter as determined by Nayfeh [33], and τ_T is a stress term due to thermal shrinkage [31], which is typical to polymer composites formed at high temperatures.

Note that in this approach the debond force, F_d, corresponding to the "kink" in the force–displacement curve (see Fig. 4), is the most important experimental quantity which is to be determined as accurately as possible.

This model also gives a direct expression for the current load, F, applied to the fiber end, as a function of the crack length

$$\begin{aligned} F &= f_s \\ &= \frac{\pi d_f}{\beta} \left\{ \tau_d \tanh[\beta(l_e - a)] - \tau_T \tanh[\beta(l_e - a)] \right. \\ &\quad \left. \times \tanh\left[\frac{[\beta(l_e - a)]}{2}\right] + \beta a \tau_f \right\}, \end{aligned} \tag{3}$$

where τ_f is the frictional stress in debonded regions, which is assumed to be independent of l_e and a.

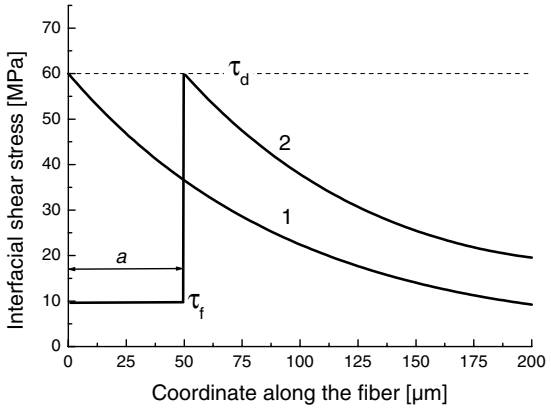

Fig. 5. Interfacial shear stress distribution along the embedded length: at the moment of crack initiation (1) and at an advanced stage of debonding when crack length is $a = 50$ μm (2).

2.3.2. Energy-controlled debonding

Some models of energy-controlled debonding can be found in [34] and [35]; the most comprehensive theory has been developed by Nairn et al. [23,26,27]. These models assume that the debonding zone extends when the energy release rate, G, reaches its critical value, G_{ic}. Thus, G_{ic} is the specific interfacial parameter in this approach, and $G = G_{ic}$ during the test. Liu and Nairn [26] derived the equation for G in a form of

$$G = g(a, l_e, F, \Delta T, \text{other factors}), \tag{4}$$

where ΔT is the temperature difference between the test temperature and the stress-free temperature, and "other factors" include interfacial friction and specimen geometry. In our previous papers, we used Eq. (4) to calculate G_{ic} from the debond force measured in pull-out and microbond experiments [24], and derived an equation

(similar to Eq. (3)) for F as a function of the crack length, with G_{ic} and τ_f as interfacial parameters [28].

Here again the debond force is the key value to be measured to calculate G_{ic}. However, both stress-based and energy-based theories of debonding allow simulation (modeling) of experimental force–displacement curves, from which further interfacial parameters, in particular, τ_f, can be determined.

2.3.3. Adhesional pressure

An interesting model of interfacial failure in a microbond and pull-out tests and a new interfacial parameter for adhesion characterization, *adhesional pressure* (σ_{ult}), were proposed by Pisanova et al. [8]. As was experimentally observed by Piggott [36] and Marotzke [37], crack initiation in these tests occurs in normal tension (Mode I). Fig. 6 schematically illustrates interfacial failure at the molecular level. Intermolecular bonds are loaded in the direction normal to the fiber surface; due to their successive breaks, the crack tip moves along the interface. The variational mechanics analysis carried out by Scheer and Nairn [27] for the microbond test showed that at crack initiation shear stress is zero at the point where the fiber enters the matrix, and the radial stress is at its maximum here (Fig. 7). This result agrees with the conclusion from the finite element analysis by Marotzke [37]. Radial stresses in microbond test geometry are shown in Fig. 8. The normal stress applied to the fiber, σ_{rr}^{f}, is directed toward the fiber axis, and the equal stress, σ_{rr}^{m}, applied to the matrix, is directed outwards. Analytical expressions derived by Scheer and Nairn allow calculating all stresses in a microbond specimen, including the radial normal stress at the interface

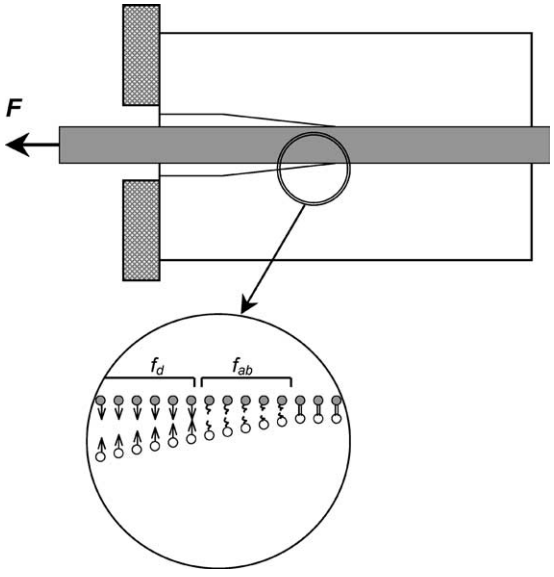

Fig. 6. Illustration of crack opening in the microbond test at the molecular level. In region f_d, only dispersion (van der Waals) forces are acting, and in region f_{ab}, both dispersion and acid–base interactions.

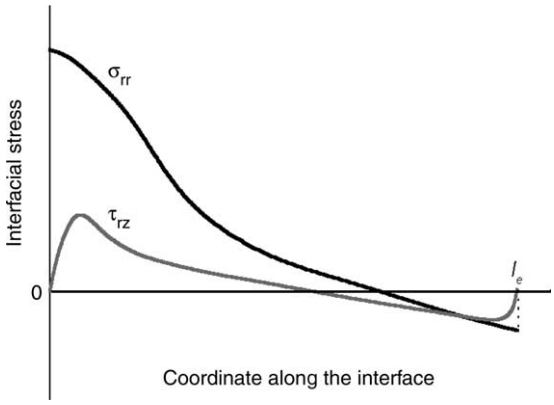

Fig. 7. Interfacial stress distribution along the embedded length in the variational mechanics model by Scheer and Nairn [27]: τ_{rz}, shear stress; σ_{rr}, radial stress.

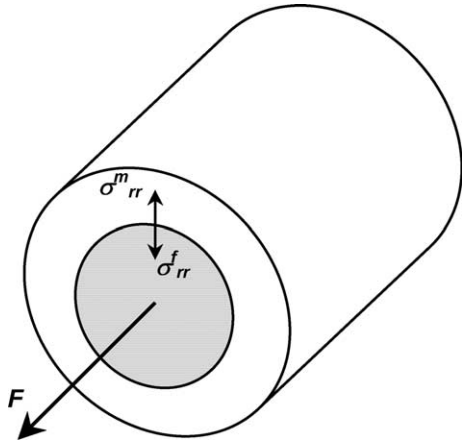

Fig. 8. Adhesional pressure in cylindrical geometry (microbond test): schematic illustration of radial stresses. Stress σ_{rr}^{m} is applied to the matrix, and σ_{rr}^{f}, to the fiber. At the moment of the onset of debonding, $\sigma_{rr}^{m} = \sigma_{rr}^{f} = \sigma_{ult}$.

which is very important for adhesion estimation. It is natural to accept the critical value of this radial normal stress (its value at the moment of crack initiation at the point where debonding starts) as a new interfacial parameter, adhesional pressure. However, we should note that (1) σ_{ult} as a failure criterion is only valid for crack initiation (at finite crack length the failure mode becomes mixed, I + II, and predominantly Mode II at large crack length); and (2) it can be calculated, strictly speaking, for the *microbond* test where the matrix undergoes compression rather than tension as in the pull-out test; all σ_{ult} data obtained using the pull-out test are only rough estimations. This is the most important difference between the pull-out and microbond tests.

The adhesional pressure is probably the most adequate parameter for characterizing the *adhesion* between the fiber and the matrix, since σ_{ult} is directly related to the thermodynamic work of adhesion between the composite constituents (see [8]). This will be discussed in more detail in Section 4.

2.3.4. Models including imperfect interface

All three models described above have been developed under the assumption that the fiber is debonded off the matrix as the interfacial crack having a sharp tip is propagating along the fiber–matrix boundary. However, it was observed that many polymer–fiber and cement–fiber systems fail under load in a more complicated manner. In particular, the front of debonding is often not localized in one point (the crack tip) but is rather a fuzzy region whose length along the fiber can be up to several fiber diameters. Within this region, partial adhesive contact between the fiber and the matrix retains (imperfect interface); full debonding takes place afterwards, behind this fuzzy zone. This behavior was experimentally observed by Piggott [36,38] for carbon fiber–epoxy matrix system. Piggott suggested a qualitative description of the mechanism of this phenomenon (multiple matrix cracking developing into "shear hackle") but did not try to derive any quantitative result. A suitable mathematical model was developed by Brameshuber et al. [25,39], who applied it to single fibers pulled from a cement matrix. This model is based on a multilinear bond law illustrated in Fig. 9, where interfacial shear stress is plotted as a function of slip (relative displacement) between the fiber and the matrix. Region I corresponds to still intact interface, Region II describes the linear stress reduction in the zone with "imperfect interface", and Region III (with constant τ) refers to fully debonded interface which transfers friction load only. The authors introduced five independent interfacial parameters which can be used for the simulation of force–displacement curves: τ_{max1} (the maximum possible shear stress in bonded regions, an analog to τ_d); s_{crit} (the maximum slip in Region I); τ_{max2} (the maximum shear stress in Region II; it can be equal to or less than τ_{max1}); n (the factor determining the maximum slip within the imperfect interface, Region II) and τ_f (frictional stress in debonded regions). In [25], the experimental force–displacement curves were fitted by theoretical ones using a five-parameter least square technique, which was time-consuming and probably might lead to ambiguous results (see the discussion in Section 4). Fortunately, this most valuable and comprehensive model can be further improved (as will be shown in Section 4) such as to allow a much simpler experimental data analysis without losing its adequacy and accuracy.

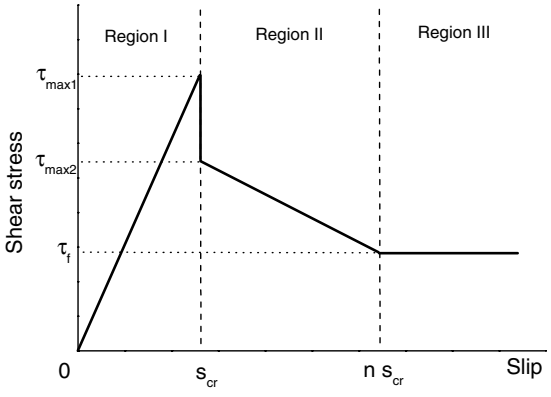

Fig. 9. Multilinear bond law used in the model with two-stage debonding (imperfect interface).

We applied all these models to determine interfacial parameters for several glass fiber–cement matrix and aramid fiber–epoxy matrix pairs, as described below. Some results concerning interfacial properties in other systems will also be discussed.

3. Experimental

3.1. Materials

The control samples of alkali resistant glass fibers (ARG) for cementitious composites have been supplied by Nippon Electric Glass Co., Ltd. (NEG ARG) and CemFIL International, Vetrotex Espana SA (VET ARG), respectively. Their major constituents determined by X-ray fluorescence spectroscopy and other general properties were published elsewhere [40].

Additional coatings were applied to improve the durability. In previous trials, styrene–butadiene dispersions were found to be most resistant in alkaline solutions. For one chemical formulation different coating concentrations were applied on NEG ARG 620-01 rovings to study the durability and the influence of the coating on the adhesion strength. Table 1 shows a summary of the coating variation and the resulting yarn tensile strength (cf. [41]). Constant contents of organic coatings were found after different alkaline treatments for VET ARG 640-02 rovings coated by same chemical formulations. Thus, the coating might save the sizing and also the ARG fibers itself. In our experiments, we used both, untreated and NaOH treated NEG ARG fibers, embedded in cementitious matrix (CEM I 52.5). According to our previous investigations [40], we selected a highly concentrated alkaline aqueous solution (5 wt% NaOH at 23 °C for 28 days, pH of 13) which proved to be the most aggressive and corrosive condition to the fiber surface out of tested ones.

Three different aramid fibers (supplied by Akzo Nobel) were investigated, indicated here as A0 (without any finish or surface treatment), A1 (with standard Twaron finish) and A2 ("adhesion activated"). The adhesion activation consisted in a proprietary treatment with an epoxy finish. DGEBA-based epoxy resin Rütapox L20 and Rütapox SL curing agent (in 100:34 weight ratio), both made and provided by Bakelite GmbH, were used to form single-fiber pull-out specimens with the aramid fibers. Some properties of the fibers and matrices used are listed in Table 2.

Table 1
Summary of sized/coated reinforcing fibers, contents of coating and yarn tensile strength

Designation	Chemistry of coating	Sizing/coating (%)	Yarn tensile strength (MPa)
NEG ARG 620-01	–	0.6/–	1351
NEG ARG 620-01/2	Styrene–butadiene1	0.6/2.4	1367
NEG ARG 620-01/2b	Styrene–butadiene1	0.6/7.0	2002

Table 2
Some properties of the fibers and the matrices used

Property	Glass fibers	Aramid fibers	Cement matrix	Epoxy matrix
Diameter, d (μm)	11–19	12	–	–
Axial modulus, E_A (GPa)	78	95	28	2.70
Transverse modulus, E_t (GPa)	78	1.9	28	2.70
Axial Poisson's ratio, ν_A	0.17	0.20	0.20	0.34
Transverse Poisson's ratio, ν_t	0.17	0.35	0.20	0.34
(Axial CTE) $\times 10^{-6}$ (K^{-1})	5	66	n/a	48
(Transverse CTE) $\times 10^{-6}$ (K^{-1})	5	–0.4	n/a	48

3.2. Pull-out test

Samples used for quasi-static single fiber pull-out tests were made by means of the technique described below. The cement/water mixture of a 0.4 ratio was placed into a special aluminum carrier and the whole unit was set into a self-made sample preparation equipment designed and constructed earlier at the Institute of Polymer Research Dresden. Two video cameras placed under optimized angles enable to visualize exactly the position of the single glass fiber to be embedded. Single fibers were end-embedded into the cement mixture perpendicularly at a PC-controlled pre-selected embedding length and exposed to curing at ambient temperature under wet conditions for about 8 h. Ten to fifteen samples prepared as described were placed after that into a desiccator at 100% RH for 7 days. Embedded lengths were chosen in the range of 200–1000 μm for quasi-static loading.

The aramid/epoxy samples were prepared in a similar way. After embedding the fiber in the matrix resin (the embedded length was in the range of 70–200 μm), the specimens were cured at 80 °C for 6 h, as recommended by the manufacturer.

The different interphases at the cementitious matrix/glass fiber interface were evaluated by single fiber pull-out test. A self-made pull-out apparatus described earlier [42] has been used for the experiments. The device allows investigators to obtain force–displacement curves of the single fiber composites under quasi-static conditions (see Fig. 4). The free fiber lengths were kept as short as possible (<0.5 mm), and the installation was stiff enough to discern the "kinks" in force–displacement curves which indicated the onset of debonding.

Single glass fibers were pulled out from the polymer matrix with a loading rate of 0.01 μm/s at ambient conditions. For aramid fibers, the pulling rate was 0.2 μm/s. The diameter of the fibers was measured immediately after the pull-out testing using an optical microscope.

3.3. Data treatment

Three techniques aimed at determining interfacial parameters (τ_f and τ_d, G_{ic}, τ_{max2}, n etc., in accord with the particular model) were used for experimental data treatment:

1. Calculating τ_d and G_{ic} from the "kink" force, F_d, for each individual force–displacement curve, using Eq. (2) and the similar equation from the energy-based debonding theory; then, calculating τ_f using the obtained τ_d value and the peak load, F_{max}, recorded for this specimen. (In fact, this second procedure is the force–displacement curve modeling using these τ_d and F_{max} values).
2. Eq. (3) gives the current load, F, applied to the fiber, as a function of the crack length, a, for a specimen with a given embedded length, l_e. Generating many $F(a)$ curves for different embedded lengths (e.g., for the range $0 < l_e \leqslant 1.5$ mm, with a 5 μm increment in l_e) and plotting their *maximum* values versus l_e, we obtain F_{max} as a function of the embedded length in the stress-based model. This function includes τ_d and τ_f as fitting parameters; using a standard least-squares method, it is possible to obtain the best fit, i.e., a pair of (τ_d, τ_f) values which minimizes the sum

$$S = \sum_i \left[F_{max}^{exper}(\tau_d, \tau_f, ...) - F_{max}^{theor}(\tau_d, \tau_f, ...)\right]^2. \quad (5)$$

We have described this procedure in detail in [31] and extended it to the energy-based model of debonding (best fit for G_{ic} and τ_f) in [28]. In this paper, the original fitting algorithm has been modified in order to take into account the scatter in individual fiber diameters.

3. Improved model originally proposed by Brameshuber et al. [25,39]. Carrying out a five-parameter least-squares analysis, as was suggested in original papers, is rather time-consuming and may yield ambiguous results. For instance, two different sets of their model parameters can produce very similar force–displacement curves, since, e.g., the variation in τ_2 can be compensated by a suitable variation in n. We modified the original model, first of all, by equating their shear-lag parameter, λ_I, to the Nayfeh's parameter, β; then, the free fiber length was determined from the slope of the initial (elastic) part of the force–displacement curve and used in further analysis (s_{cr} can be calculated using the known β value); the τ_d value was calculated from the "kink" force, and τ_f, from the region corresponding to post-debonding friction; and, finally, τ_2 and n were determined using a least-squares method (by fitting the experimental pull-out curve) with only these two fitting parameters. This new procedure is described in details in [43]. Here we should note that τ_d in this model has different physical meaning than τ_d in traditional stress-based models of debonding, since it corresponds to the beginning of the second stage of debonding ("bond softening") rather than full debonding.

4. Results and discussion

4.1. "Kink" force versus two-parameter fit

Tables 3 and 4 compare the τ_d and τ_f values (for glass fiber–cement matrix and aramid fiber–epoxy matrix systems, respectively) calculated within the frames of the stress-based model using individual force–displacement curves (with F_d and F_{max} as key experimental data, see Section 3.3, item 1) and using a two-parameter least squares method to fit experimentally obtained $F_{max}(l_e)$ relationships by theoretical functions (Section 3.3, item 2). In Tables 5 and 6, energy-based interfacial parameters for these systems (G_{ic} and τ_f) are presented and compared.

First of all, we should note that the local interfacial shear strength (τ_d) values, calculated from the "kink"

Table 3
Local interfacial shear strength (τ_d) and interfacial frictional stress (τ_f) in NEG fibers–cement matrix systems estimated using individual force–displacement curves (1) and two-parameter fit of the maximum force as a function of embedded length (2)

Fibers		NEG ARG 620-01		NEG ARG 620-01/2		NEG ARG 620-01/2b	
		τ_d (MPa)	τ_f (MPa)	τ_d (MPa)	τ_f (MPa)	τ_d (MPa)	τ_f (MPa)
Untreated	1	23.3 ± 8.0	4.6 ± 1.9	34.1 ± 11.0	3.3 ± 1.7	25.1 ± 11.2	1.3 ± 1.0
	2	60.8	2.43	91.8	0.22	–	–
NaOH treated	1	28.16.4	1.7 ± 0.4	39.6 ± 11.7	5.1 ± 2.5	38.9 ± 10.8	3.2 ± 1.5
	2	40.3	0.93	88.1	0.80	30.9	3.46

Table 4
Local interfacial shear strength (τ_d) and interfacial frictional stress (τ_f) in aramid fibers–epoxy matrix systems estimated using individual force–displacement curves (1) and two-parameter fit of the maximum force as a function of embedded length (2)

Fibers	Aramid A0		Aramid A1		Aramid A2	
	τ_d (MPa)	τ_f (MPa)	τ_d (MPa)	τ_f (MPa)	τ_d (MPa)	τ_f (MPa)
1	49.7 ± 8.9	18.8 ± 7.3	41.8 ± 8.9	17.2 ± 6.9	59.0 ± 11.2	25.8 ± 13.2
2	67.8	7.0	60.3	4.4	71.8	8.6

Table 5
Critical energy release rate (G_{ic}) and interfacial frictional stress (τ_f) in NEG fibers–cement matrix systems estimated using individual force–displacement curves (1) and two-parameter fit of the maximum force as a function of embedded length (2)

Fibers		NEG ARG 620-01		NEG ARG 620-01/2		NEG ARG 620-01/2b	
		G_{ic} (J/m^2)	τ_f (MPa)	G_{ic} (J/m^2)	τ_f (MPa)	G_{ic} (J/m^2)	τ_f (MPa)
Untreated	1	0.60 ± 0.07	4.6 ± 1.9	1.29 ± 0.10	3.3 ± 1.7	0.70 ± 0.12	1.3 ± 1.0
	2	4.0	2.6	10.4	0.4	–	–
NaOH treated	1	0.87 ± 0.06	1.7 ± 0.4	1.74 ± 0.11	5.1 ± 2.5	1.68 ± 0.09	3.2 ± 1.5
	2	1.8	0.83	8.3	0.78	–	–

Table 6
Critical energy release rate (G_{ic}) and interfacial frictional stress (τ_f) in aramid fibers–epoxy matrix systems estimated using individual force–displacement curves (1) and two-parameter fit of the maximum force as a function of embedded length (2)

Fibers	Aramid A0		Aramid A1		Aramid A2	
	G_{ic} (J/m^2)	τ_f (MPa)	G_{ic} (J/m^2)	τ_f (MPa)	G_{ic} (J/m^2)	τ_f (MPa)
1	14.3 ± 0.9	18.8 ± 7.3	12.1 ± 1.0	17.2 ± 6.9	20.6 ± 1.4	25.8 ± 13.2
2	26.6	8.1	21.0	4.6	29.8	9.2

force, seem to be quite plausible. For aramid–epoxy systems, these are close to the tensile strength of the matrix, which is corroborated by the fact that the aramid–epoxy interface was reported to fail in the mixed (adhesive + cohesive) mode [44]. For glass fibers combined with cement matrices, the local interfacial shear strength is somewhat smaller, which indicates weaker physicochemical bonding between the fiber surface and the matrix and can be due, in part, to the presence of voids near the interface. The τ_f values, determined using this method, for all systems are in good agreement (within 20% error) with the frictional stress estimated from the post-debonding regions of the force–displacement curves, which further evidences the accuracy of the technique used.

Since the derivation of the critical energy release rate, G_{ic}, from F_d values is based on the same principles and assumption on which the τ_d calculation is based (cf. [27,28]) and G_{ic} and τ_d are related by a (polynomial) function [24,28], G_{ic} values in Tables 5 and 6, calculated from individual force–displacement curves, can also be regarded as reliable. For aramid–epoxy systems, the critical energy release rate was much greater than for glass fiber–cement composites, which can be attributed to both very high level of interfacial adhesion between the aramid fiber and epoxy and higher deformability of the epoxy matrix. As for frictional stress values, these are practically identical to those obtained using the stress-based approach.

Fig. 10 shows typical plots of the maximum pull-out force, F_{max}, and the apparent interfacial shear strength, τ_{app} (see Eq. (1)), versus the embedded length. The experimental data display well-known theoretical behavior (F_{max} increases with l_e, but at the same time τ_{app} increases when $l_e \to 0$), but show rather large scatter. This was typical for both fiber–matrix systems studied and all fiber treatments. As a result, the two-parameter least squares fit was, under such conditions, very inaccurate: the error in τ_d, G_{ic} and τ_f (not shown in Tables 3–6) was comparable with their nominal average values. This can be illustrated by a sum of least squares map plotted for the same pull-out data set as in Fig. 10(b), i.e., aramid A2–epoxy (Fig. 11). As can be seen, this map presents a narrow valley with steeply rising banks but very slow variation in height along the valley itself. Thus, the minimum appears to be very shallow. The point which represents the mean τ_d and τ_f values calculated from the debond force in individual specimens falls in the valley, but if the number of specimens is small, it often does not correspond to the point resulting from the two-parameter best fit. As we know from our own experience, these two points are close only for a large number of specimens (about 100). Small distance between these points can be regarded as an indication of "good" statistics and sufficient reliability of the result. In any case, one should prefer the mean value from individual experiments in which F_d values were determined directly. If the equipment does not allow the F_d measurement and only F_{max} values are reliable, at least 100 specimens should be tested. However, we should mention that in this case the two-parameter fit technique

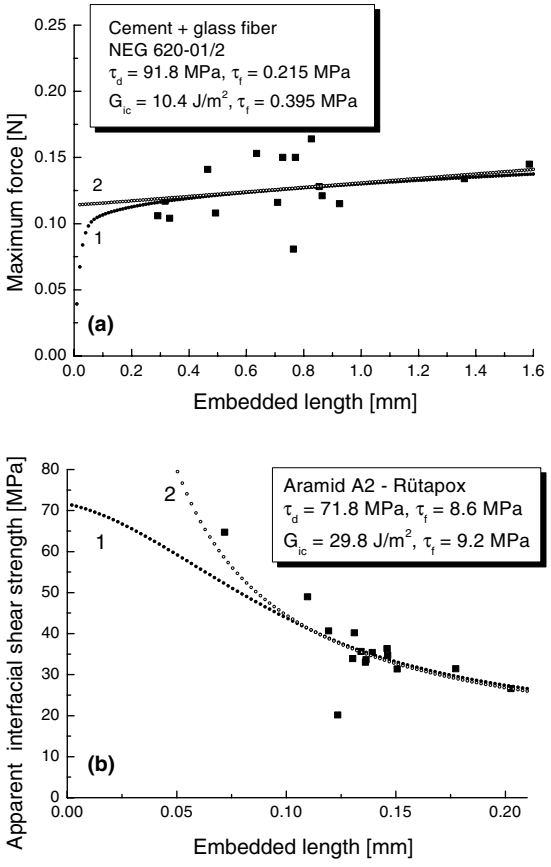

Fig. 10. The maximum pull-out force (a) and the apparent interfacial shear strength (b) plotted as functions of the embedded length. Curves 1 are stress-based two-parameter best fits, and curves 2 are energy-based best fits.

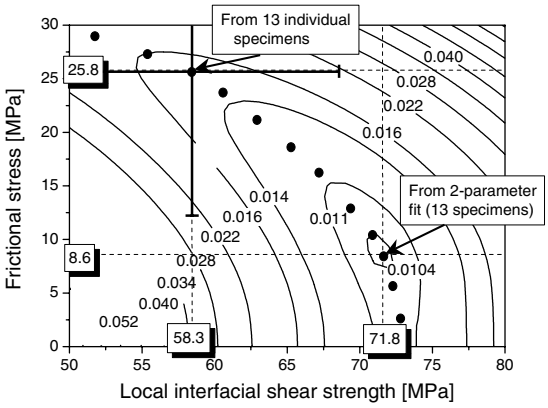

Fig. 11. The map of the sum of least squares (in arbitrary units) as a function of the local bond strength, τ_d, and the frictional stress, τ_f, for Aramid A2–Rütapox system. For the mean value determined from 13 individual specimens, SDs in τ_d and τ_f are shown.

gives quite good results for both stress-based and energy-based models of interfacial debonding [28,31].

Additional factor that can affect the accuracy of the technique based on the maximum pull-out force as a function of the embedded length is possible non-elastic interface behavior at advanced stages of the test, i.e., after the debonding initiation. Larger loads applied to the fiber can cause plastic deformation of the matrix and/or alternative mechanisms of the matrix failure near the interface [36,38]. In any case, an adequate technique of bond strength determination in single fiber pull-out test must be based on the measurement at a rather low external load, such as F_d – or, alternatively, explicitly include non-elastic effects.

4.2. Modeling of a force–displacement curve for an imperfect interface

A model pretending to adequately consider stress transfer through the interface and interfacial failure must include a realistic law of interfacial interaction. Of course, it is extremely difficult to take into account all physical and chemical interactions taking place between two dissimilar phases in contact; therefore, any model proposing a reasonable approximation to real bond law should be considered with proper attention.

The model proposed by Brameshuber et al. [25,39] seems to be an important step to deeper insight into mechanics of interfaces. It uses a multilinear bond law whose three regions include elastic behavior for intact interface, bond softening with progressive breaking of adhesive bonds, and post-debonding friction. The multilinear law implies additional interfacial parameters (the model has five parameters) which, in turn, allows for additional degrees of freedom. And the remarkable feature of this model is that it can easily be related to, or combined with, a traditional "elastic" model to clarify the physical meaning of its parameters.

We used this model in a modified form, combining it with an "elastic" stress-based shear-lag consideration. Our approach can be illustrated by the procedure of fitting an experimental force–displacement curve (see Fig. 12), which we used instead of a standard five-parameter least squares fit as recommended by the authors. The data treatment procedure is described in Section 3. The τ_d and τ_f values are close to those obtained using an elastic approach (Section 3.3). The effective free fiber length (including the true fiber length plus fiber deformation within the glue droplet by which it was fixed to the test installation) was estimated to be equal to 0.48 mm. The model allows estimation of "inelastic" parameters (τ_{max2} and n) which help to characterize, respectively, the "degree of perfection" ($\tau_{max2}/\tau_d = 0.88$) and the deformability at the second stage of debonding. This model can be very useful for interface investigation in cementitious composites, as well as for re-evaluating experimental data on polymer–fiber systems whose behavior cannot be satisfactorily described by traditional elastic models.

4.3. Adhesional pressure and the effective interphase thickness

We consider the processes, which take place at the fiber–matrix interface during the crack opening, at two structural levels.

At the molecular level, the work equal to the work of adhesion is to be done in order to separate a unit area of the fiber surface from the matrix. This work is done against the adhesional pressure and is proportional to it:

$$W_A = \lambda \cdot \sigma_{ult}. \quad (6)$$

The coefficient of proportionality, λ, is the effective range of action of intermolecular forces [8,20], which depends on the chemical nature of the fiber and the matrix. Having independently determined the adhesional pressure according to the approach proposed by Scheer and Nairn [27] (a detailed, step-by-step algorithm was de-

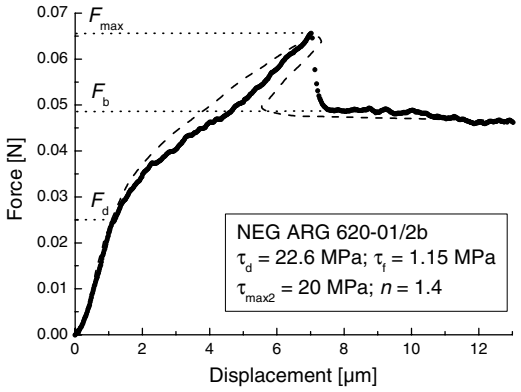

Fig. 12. The experimental force–displacement curve for glass fiber–cement matrix specimen (black points/solid line) and its fit according to the model by Brameshuber et al. [25,39] (dash line).

Table 7
Adhesional parameters and interphase characteristics for some fiber–polymer systems

Fiber	Matrix	τ_d (MPa)	σ_{ult} (MPa)	G_{ic} (J/m^2)	W_A (J/m^2)	λ (Å)	d (μm)
Carbon T300	Nylon 6,6	25.4	132.4	11.0	0.0933	7.05	0.083
E-glass	Nylon 6,6	88	208.2	34.5	0.1088	5.23	0.166
E-glass	Polystyrene	94	192.5	44	0.1121	5.82	0.229
E-glass	Polypropylene	13.5	99.8	4.7	0.0673	6.74	0.047
E-glass	Polyethylene	14.6	81.4	5.7	0.0680	8.35	0.070
E-glass	Polycarbonate	92	276.6	57	0.1116	4.03	0.206

τ_d, local interfacial shear strength; σ_{ult}, adhesional pressure; G_{ic}, critical energy release rate for crack initiation (all three parameters determined from the microbond test).
W_A, work of adhesion (calculated from IGC experiments). $\lambda = W_A/\sigma_{ult}$, range of action of intermolecular forces at the interface; $d = G_{ic}/\sigma_{ult}$, effective thickness of the interphase.

scribed in [8]) and the work of adhesion (e.g., using the inverse gas chromatography technique [7,45,46]), we can calculate λ for a given fiber–matrix pair. To illustrate this, we used the results published in our prior paper [8]. Table 7 presents the σ_{ult}, W_A and λ values for several glass fiber–polymer and carbon fiber–polymer systems. As could be expected, the λ values are of an order of 4–9 Å and correspond well to the ranges of action of molecular forces.

However, if we consider the crack opening at the micro level, we note that a much larger work than W_A, namely, the work equal to the critical energy release rate, G_{ic}, is required to start interfacial debonding. The G_{ic} values are by 2–3 orders of magnitude greater than the W_A values for the same systems. This is due to the fact that relatively thick regions in the matrix and the fiber, not just two contacting monomolecular layers, are involved in deformation produced by the external load. Writing an equation similar to (6) but involving G_{ic} instead of W_A,

$$G_{ic} = d \cdot \sigma_{ult}, \tag{7}$$

we can conclude that d in this equation is the effective deformation of the fiber and matrix layers adjacent to the interface, or, in other words, the thickness of the "interphase" involved in load transfer. Using our σ_{ult} and G_{ic} values listed in Table 7 (the latter were calculated from our own raw data also used by us to calculate σ_{ult} in [8]), we determined the interphase thickness for all mentioned polymer–fiber pairs. We should emphasize again that G_{ic} values for these calculations should be taken at the moment of crack initiation in the pull-out or microbond test, when the failure mode is Mode I and, thus, the G_{ic} value characterizes essentially tensile (not shear) deformation. In addition, the order of magnitude of the calculated thickness is in a good agreement with experimental results determined using Force Volume Nanoindentation technique [47].

5. Conclusion

We have compared various approaches to the characterization of the strength of fiber–matrix interfaces, based on micromechanical (single fiber) tests. Both, energy-based (critical energy release rate) and stress-based (local interfacial shear strength) criteria can be successfully used as interfacial parameters. An interesting and important parameter is the adhesional pressure, which is a natural stress-based criterion of interfacial failure. Using adhesional pressure, we can directly relate "practical" adhesion (bond strength) to "fundamental" adhesion (work of adhesion) and estimate the thickness of the effectively loaded interphase.

The use of the debond force for determining adhesion parameters and both, debond and maximum force to estimate interfacial friction, gives the best results for both, polymeric and cementitious composites. Two-parameter fit is a simple and quick technique but it can only be used when the number of specimens tested is large enough. Models with imperfect interface are the most comprehensive but hardly applicable to real micromechanical tests, because they contain too many fitting parameters. However, these models can be significantly improved by further development and yield good results for the systems in which debonding is accompanied by matrix failure, i.e., cement-based composites and polymer composites with high interfacial adhesion and relatively ductile matrices.

Acknowledgement

The authors acknowledge the technical assistance of Alma Rothe.

References

[1] Mittal KL. Adhesion measurement of films and coatings: a commentary. In: Mittal KL, editor. Adhesion measurement of films and coatings. Utrecht, The Netherlands: VSP; 1995. p. 1–13.
[2] Fowkes FM. Role of acid–base interfacial bonding in adhesion. J Adhesion Sci Technol 1987;1:7–27.
[3] Drzal LT, Sugiura N, Hook D. The role of chemical bonding and surface topography in adhesion between carbon fibers and epoxy matrices. Compos Interfaces 1997;4:337–54.

[4] Favre JP, Désarmot G, Sudre O, Vassel A. Were McGarry or Shiriajeva right to measure glass–fiber adhesion?. Compos Interfaces 1997;4:313–26.
[5] Good RJ. Contact angle, wetting, and adhesion: a critical review. In: Mittal KL, editor. Contact angle, wettability and adhesion. Zeist, The Netherlands: VSP; 1993. p. 3–36.
[6] Désarmot G, Favre JP. Advances in pull-out testing and data analysis. Compos Sci Technol 1991;42:151–87.
[7] Nardin M, Schultz J. Relationship between fiber–matrix adhesion and the interfacial shear strength in polymer-based composites. Compos Interfaces 1993;1:172–92.
[8] Pisanova E, Zhandarov S, Mäder E. How can adhesion be determined from micromechanical tests?. Compos Part A 2001;32:425–34.
[9] Penn LS, Bowler ER. A new approach to surface energy characterization for adhesive performance prediction. Surf Interfac Anal 1981;3:161–4.
[10] Miller B, Muri P, Rebenfeld L. A microbond method for determination of the shear strength of a fiber–resin interface. Compos Sci Technol 1987;28:17–32.
[11] Gorbatkina YA. Adhesive strength of fiber–polymer systems. New York: Ellis Horwood; 1992.
[12] Tandon GP, Pagano NJ. Micromechanical analysis of the fiber push-out and re-push test. Compos Sci Technol 1998;58:1709–25.
[13] Kerans RJ, Parthasarathy TA. Theoretical analysis of the fiber pullout and pushout tests. J Am Ceram Soc 1991;74:1585–96.
[14] Kelly A, Tyson WR. Tensile properties of fibre-reinforced metals – copper/tungsten and copper/molybdenum. J Mech Phys Solids 1965;13:329–50.
[15] Broutman L. Measurement of fiber–polymer matrix interfacial strength. In: Interfaces Compos STP-452. Philadelphia, PA: American Society for Testing and Materials; 1969. p. 27–41.
[16] Nairn JA, Liu YC. On the use of energy methods for interpretation of results from single-fiber fragmentation experiments. Compos Interfaces 1996;4:241–67.
[17] Feillard P, Désarmot G, Favre JP. A critical assessment of the fragmentation test for glass/epoxy systems. Compos Sci Technol 1993;49:109–19.
[18] Henstenburg RB, Phoenix SL. Interfacial shear strength studies using the single-filament-composite test: II. A probability model and Monte Carlo simulation. Polym Compos 1989;10:390–408.
[19] Zhandarov SF, Pisanova EV. Two approaches to interfacial shear strength calculation based on the single fibre composite test. Mech Compos Mater 1995;31:446–61.
[20] Nardin M, Schultz J. Relationship between work of adhesion and equilibrium interatomic distance at the interface. Langmuir 1996;12:4238–42.
[21] Pisanova E, Zhandarov S. Reversible and irreversible adhesion of polymers: possibilities for measurement and calculation. J Adhesion 2001;75:89–127.
[22] Zhandarov S, Pisanova E, Schneider K. Fiber-stretching test: a new technique for characterizing the fiber–matrix interface using direct observation of crack initiation and propagation. J Adhesion Sci Technol 2000;14:381–98.
[23] Nairn JA. Analytical fracture mechanics analysis of the pull-out test including the effects of friction and thermal stresses. Adv Compos Lett 2000;9:373–83.
[24] Zhandarov S, Pisanova E, Mäder E. Is there any contradiction between the stress and energy failure criteria in micromechanical tests? Part II Crack propagation: effect of friction on force–displacement curves. Compos Interfaces 2000;7:149–75.
[25] Brameshuber W, Banholzer B. Eine Methode zur Beschreibung des Verbundes zwischen Faser und zementgebundener Matrix. Beton- und Stahlbetonbau 2001;96:663–9.
[26] Liu CH, Nairn JA. Analytical fracture mechanics of the microbond test including the effects of friction and thermal stresses. Int J Adhesion Adhesives 1999;19:59–70.
[27] Scheer RJ, Nairn JA. A comparison of several fracture mechanics methods for measuring interfacial toughness with microbond tests. J Adhesion 1995;53:45–68.
[28] Zhandarov S, Mäder E. Indirect estimation of fiber/polymer bond strength and interfacial friction from maximum load values recorded in the microbond and pull-out tests. Part II: Critical energy release rate. J Adhesion Sci Technol 2003;17:967–80.
[29] Leung CKY, Li VC. New strength-based model for the debonding of discontinuous fibers in an elastic matrix. J Mater Sci 1991;26:5996–6010.
[30] Kanda T, Li VC. Interface property and apparent strength of high-strength hydrophilic fiber in cement matrix. J Mater Civil Eng 1998;10:5–13.
[31] Zhandarov SF, Mäder E, Yurkevich OR. Indirect estimation of fiber/polymer bond strength and interfacial friction from maximum load values recorded in the microbond and pull-out tests. Part I: Local bond strength. J Adhesion Sci Technol 2002;16:1171–200.
[32] Zhandarov SF, Pisanova EV. The local bond strength and its determination by the fragmentation and pull-out tests. Compos Sci Technol 1997;57:957–64.
[33] Nayfeh AH. Thermomechanically induced interfacial stresses in fibrous composites. Fibre Sci Technol 1977;10:195–209.
[34] Leung CKY. Fracture-based two-way debonding model for discontinuous fibers in an elastic matrix. J Eng Mech 1992;118:2298–318.
[35] Stang H, Shah SP. Failure of fiber reinforced composites by pull-out fracture. J Mater Sci 1986;21:953–8.
[36] Piggott MR. A new model for interface failure in fibre-reinforced polymers. Compos Sci Technol 1995;55:269–76.
[37] Marotzke C. Influence of the fiber length on the stress transfer from glass and carbon fibers into a thermoplastic matrix in the pull-out test. Compos Interfaces 1993;1:153–66.
[38] Piggott MR. Why interface testing by single-fibre methods can be misleading. Compos Sci Technol 1997;57:965–74.
[39] Brameshuber W, Banholzer B, Brümmer G. Ansatz für eine vereinfachte Auswertung von Faser-Ausziehversuchen. Beton- und Stahlbetonbau 2000;95:702–6.
[40] Gao SL, Mäder E, Abdkader A, Offermann P. Sizings on alkali-resistant glass fibers: environmental effects on mechanical properties. Langmuir 2003;19:2496–506.
[41] Mäder E, Plonka R, Schiekel M, Hempel R. Coatings on alkali-resistant glass fibres for the improvement of concrete. J Indust Textiles 2004;33:191–207.
[42] Mäder E, Grundke K, Jacobasch HJ, Panzer U. Interphase characterization in reinforced polymers. In: Proceedings of 31st international man-made fibre congress, Dornbirn, Austria; 1989.
[43] Zhandarov S, Mäder E. Determination of interfacial parameters in fiber-polymer systems from pull-out test data using a bilinear bond law. Compos Interfaces 2004 (in press).
[44] Pisanova E, Zhandarov S, Mäder E, Ahmad I, Young RJ. Three techniques of interfacial bond strength estimation from direct observation of crack initiation and propagation in polymer–fibre systems. Compos Part A 2001;32:435–43.
[45] Jacobasch HJ, Grundke K, Mäder E, Freitag KH, Panzer U. Application of the surface energy concept in polymer processing. J Adhesion Sci Technol 1992;6:1381–96.
[46] Lloyd DR, Ward TC, Schreiber HP, editors. Inverse gas chromatography: characterization of polymers and other materials. ACS Symposium Series, 391. Washington, DC: American Chemical Society; 1989.
[47] Gao SL, Mäder E, Plonka R. Mapping composite interphase properties – elasticity and electricity. In: Proceedings of conference on interfaces and interphases in multicomponent materials, Balatonfüred, Hungary; October 5–8, 2003.